Electrodeposition of nanostructured bioactive hydroxyapatite-heparin composite coatings on titanium for dental implant applications

Benedetto Bozzini · Amilcare Barca · Francesco Bogani · Marco Boniardi · Paolo Carlino · Claudio Mele · Tiziano Verri · Alessandro Romano

Received: 10 July 2013 / Accepted: 17 February 2014 / Published online: 12 March 2014

1 Introduction

Titanium and titanium-based alloys are the materials of choice for load-bearing implants in clinical dentistry, owing to their optimal mechanical properties and corrosion resistance [1] as well as to the remarkable biocompatibility of the stable oxides that form on their surfaces [2, 3]. Recent studies disclosed the possibility of fabricating zirconium implants, similar to titanium as far as their mechanical properties are concerned, coated with ZrO_2 in order to combine the advantages of biocompatibility of the ceramic coating with the strength and toughness of the bulk metal [4]. However, at present, titanium-based endosseous implants are the only ones used in surgical practice. In order to enhance bioactivity and osteointegration, hydroxyapatite (HA, $Ca_{10}(PO_4)_6(OH)_2$) has been widely employed as a coating material for titanium, due to its chemical similarity with natural bone tissue and high biocompatibility [1, 2, 5–7]. Several methods—such as plasma spray, sol–gel, electrophoretic, radio frequency sputtering and electrochemical deposition—have been proposed to coat implant surfaces [5, 8]. Among these methods, electrodeposition is a relatively inexpensive, green and energy saving process, allowing to obtain controlled micro- and nanometric structures [2, 9–14]. Biocompatibility is favoured by the porous structure achieved by electrodeposition, assuring a better contact with the bone tissue since it exhibits a notably larger active surface with respect to the prosthesis substrate, and promoting adhesion and stability [15–17]. The field of HA electrodeposition on Ti has been thoroughly reviewed in [18], covering in detail the following aspects: (i) electrodeposition mechanism and bath chemistries; (ii) Ti-based substrate pretreatments and coating post-treatments; (iv) structural and morphological characterisation of the HA films, with special emphasis on nanostructuring; (v) biocompatibility assays.

The contact of biomaterials with blood triggers multiple pathophysiological defensive actions (activation of the coagulation cascade, platelet adhesion, activation of the complement system, etc.). The reduction of these events is

B. Bozzini (✉) · F. Bogani · P. Carlino · C. Mele
Dipartimento di Ingegneria dell'Innovazione, Università del Salento, via Monteroni, 73100 Lecce, Italy
e-mail: benedetto.bozzini@unisalento.it

A. Barca · T. Verri · A. Romano
Dipartimento di Scienze e Tecnologie Biologiche e Ambientali, Università del Salento, via Monteroni, 73100 Lecce, Italy

M. Boniardi
Dipartimento di Meccanica, Politecnico di Milano, via La Masa 1, 20156 Milan, Italy

crucial for the successful performance of a biomedical device (see e.g. [19]). Thus, improving the blood compatibility of a material can lead to effective enhancement of overall biocompatibility. In particular, enhancing the anticoagulant properties of the implant materials by proper functionalization is necessary to reduce the activation of the coagulation process itself and/or alter other health states such as the local tissue destruction due to peri-implantitis, one of major concerns in implant dentistry today. The blood compatibility of HA can be improved by incorporation of heparin into the HA coatings, resulting in e.g. an antithrombogenic biomaterial [20, 21]. In fact, heparin, a member of a family of polyanionic polysaccharides called glycosaminoglycans (see e.g. [22, 23]), exhibits among many others—strong anticoagulant properties, thus representing one of the major anticoagulant drugs (see e.g. [24–26], and literature cited therein). Because of its anticoagulant properties, heparin has widely been used for the surface modification of biomedical implants to improve blood compatibility [20, 27–29], where it can efficiently be integrated either directly or indirectly via e.g. heparin-binding peptides (see e.g. [30, 31]).

In this work we propose an innovative electrodeposition method: the one-pot fabrication of pure HA coatings and HA-heparin composites on Ti substrates, without need of post-treatments. HA and HA-heparin coatings have been characterised from the chemical, morphological and structural points of view. In addition, the quantity of the electrodeposited heparin on Ti substrate has been investigated and the effect of the HA and HA-heparin coatings on cell proliferation/viability has been evaluated.

2 Materials and methods

Commercial pure titanium 20 × 15 × 1 mm^3 foils (Goodfellow 99.6 + %) were used as substrates. The specimens were polished with 1200# abrasive papers, cleaned with acetone under ultrasound agitation, rinsed with distilled water and dried in a N_2 flow. Since the impact of Ti roughness and porosity on osteointegration is well known to be crucial [32–36], and in typical cases of clinical interest the impant response is entirely controlled by the mechanical surface finishing [37–40], we decided to concentrate on the coating and, in order to single out just its effects, we worked with Ti substrates exhibiting a well-defined and reproducible surface finish. The electrolyte used for the electrodeposition of calcium phosphate coatings was prepared by dissolving reagent-grade 0.61 mM $Ca(NO_3)_2$ and 0.36 mM $NH_4H_2PO_4$ in ultrapure water with a resistivity of 18 MΩ from a Millipure Milli-Q system, according to the recipe proposed in [15]. In order to enhance cathodic base formation, 0.1 M $NaNO_3$ was added. The pH of the electrolyte was adjusted with NaOH at a value of 6.0 so that the electrolyte was saturated with respect to HA [15]. Sodic heparin (Vister) at three different concentrations, 0.5, 1.7 and 5.0 g L^{-1}, was also added to obtain a composite featuring improved hemocompatibility [28, 29]. The use of deaerated solutions is recommended for the growth of HA [2, 9–14]. In the specific case, as detailed below in the Section dealing with SEM, we have employed boiling aqueous solutions, that did not require external deaeration.

Electrochemical measurements (linear sweep voltammetry, potentiostatic deposition) were carried out with an AMEL 5000 potentiostat/galvanostat, employing a three-electrode electrochemical cell. The counter electrode (CE) was a platinised Ti expanded mesh electrode exhibiting an area of ca. 5 cm^2 and the reference electrode (RE) was an AMEL Ag/AgCl (KCl 3 M); potential values are reported versus Ag/AgCl. The surface morphology of the coatings was examined with a Cambridge Stereoscan scanning electron microscope (SEM). The crystallographic structure of the coatings was investigated using an X-ray Ultima + Rigaku diffractometer, equipped with a Bragg–Brentano goniometer. The thickness of the electrodeposited coatings was estimated using a UVISEL Spectroscopic Ellipsometer with polariser and incidence angles of 60°. Reflectivity in 8 different points of each sample and for several deposition times has been measured at a wavelength of 450 nm, where titanium exhibits a high reflectivity [41].

Complementary shear and scratch adhesion testing methods were employed for the evaluation of the adhesion resistance of the coatings. Shear adhesion strength of the electro-deposited HA-coatings was tested following the ASTM F1044-05 Standard, as recommended in [42, 43]. During the measurements, the titanium sheets were bonded to both the coated and the uncoated side of each samples using epoxy glue (model DP410 Scotch-weld, 3 M), whose measured shear strength was about 36 MPa (±2 MPa). Tensile tests were carried out on a universal testing machine (MTS model 45, load cell: 10 kN) with a crosshead speed of 0.8 mm/min. Shear strengths were calculated as peak forces versus fracture areas. Special care was taken in order to avoid epoxy resin penetration through coating macropores, since this phenomenon would result in partial bonding to the substrate, yielding false adhesion data. Scratch tests were performed in order to evaluate the coating adhesion as a function of coating deposition method [44]. Three coated specimens were scratched using a CSM testing machine, mod. MCT/SN 50-0223 (preload: 1 N, maximum load 30 N, load speed of 12.5 N min^{-1}) according to the ASTM C1624 standard. Scratch lines were measured by SEM (Cambridge Stereoscan 360) to determine the critical scratch loads and to allow the calculation of the coating shear stresses.

Heparin incorporation into the coatings electrodeposited onto titanium was assessed using qualitative Alcian Blue

staining [45]. Briefly, the samples were stained for 30 min using a solution of Alcian Blue 8GX (2 % w/v) acetic acid (3 % v/v). After staining, the samples were washed thoroughly with demineralised water for 15 min and observed using a Nikon AZ100 Multizoom Microscope equipped with DIC optics. The amount of electrodeposited heparin was determined using toluidine blue assay [46]. The rectangular titanium foils were incubated with 3 ml of a freshly prepared solution of toluidine blue (0.01 M HCl, 2 mg mL^{-1} NaCl, 0.4 mg/ml toluidine blue O zinc chloride double salt; TBO assay) for 4 h at room temperature to form the heparin–toluidine blue complex on the sample surface. Subsequently, the foils were washed twice (for 5 min) with demineralised water and incubated with 3 ml of a 1:4 (v/v) mixture of 0.1 M NaOH and ethanol to solubilise the heparin–toluidine blue complex. After complete dissolution of the complex, bringing about the complete decolourisation of the samples, the absorbance of the resulting solutions was measured at 530 nm using a Beckman Coulter DU® 640B spectrophotometer. The amount of electrodeposited heparin was calculated from a calibration curve constructed using various concentrations of heparin.

HeLa cells from human tumoral endometrium were cultured in Dulbecco's modified Eagle's medium (DMEM) supplemented with 10 % heat-inactivated fetal bovine serum, 0.1 mg mL^{-1} streptomycin, 100 U mL^{-1} penicillin. Cells were maintained at 37 °C and 5 % CO_2 in a humidified incubator. The effects of the surface coatings on proliferation of HeLa cells were investigated by MTT assay. This method is based on the reduction of 3-[4,5-dimethylthiazol-2-yl]-2,5-diphenyl tetrazolium (MTT) salt by mitochondrial dehydrogenases of viable cells to a purple formazan product [47]. Briefly, the cells were seeded onto uncoated (control) or coated (HA or HA-heparin) Ti surface at a density of 2×10^4 cells cm^{-2} and incubated for 48 h. MTT was added at a final concentration of 0.5 mg mL^{-1} 4 h before termination of the incubation. The purple formazan formed by viable cells was extracted with acidified isopropanol and the absorbance of the dye was measured spectrophotometrically at 570 nm. The measured optical density was used to calculate cell viability, expressed as the percentage with respect to the control sample (uncoated Ti surface). For the statistical analysis of the data the Bonferroni post hoc test was used and a P value <0.05 was considered significant. All the results are the mean of three experiments. The morphology of HeLa cells was examined using acridine orange (AO) staining. Cells were cultured for 48 h on the surface of uncoated Ti (control) foils and on HA and HA-heparin coated Ti foils. Then, the cells were washed twice with phosphate buffered saline (PBS), fixed with freshly prepared 2 % paraformaldehyde for 30 min at room temperature, washed twice with PBS and finally stained with 10 μg mL^{-1} AO for 15 min. After staining, the cells were washed with water and observed with a fluorescence microscope (Nikon AZ100 Multizoom) equipped with blue excitation filter (B-2A).

3 Results and discussion

3.1 Electrochemical processing conditions and electrokinetics

Process optimisation, based on the morphological, structural and growth rate results detailed in the corresponding Sections of this paper, yielded the following deposition conditions: potentiostatic deposition of 2 h at −1.4 V versus Ag/AgCl, boiling solution, heparin concentration is 1.7 g L^{-1}. The specific reasons why these conditions were identified as optimal will be discussed where relevant. Essentially, the choice of temperature and lower-heparin concentration range is dictated by the impact of the processing conditions on nanowire formation—described in the Section commenting the SEM results—and the selection of the particular concentration of 1.7 g L^{-1} is motivated by the fact that it yields the maximum heparin incorporation into the composite—as expoundended in the Section reporting the staining measurements. The growth rate has been evaluated by the spectroellipsometric method [48], in correspondence of several deposition times, in 8 different points of the samples, chosen in order to offset possible current density distribution effects. Calibration of the optical response with respect to thickness was performed by means of a Talystep line profilometer. The experimental optical parameters derived from optically thick HA ad HA-heparin samples and clean Ti substrates were implemented in an two-layer optical model—including an HA or HA-heparin layer on Ti substrate, solved numerically with the Deltapsi II program (for details, see [49]), incorporating roughness effects [50], for the accurate estimation of the sample thickness. The model results were cross-checked with simulations performed with literature optical data for HA onto Ti [41, 51–54] and found to match accurately. The thickness of HA and HA-heparin coatings as a function of deposition time is reported in Fig. 1. Slightly thicker coatings have been obtained in the presence of heparin at the highest investigated electrodeposition times, coherently with literature results reporting an enhancement of deposition rate brought about by the addition of heparin in cognate systems [21].

In order to assess the electrokinetic contribution of each bath constituent to the base generation process, we measured cathodic linear sweep voltammograms (LSVs, Fig. 2) at a scan rate of 1 mV s^{-1} at Ti electrodes in contact with the following solutions at pH 6.0 adjusted with HCl, each in the presence and in the absence of heparin:

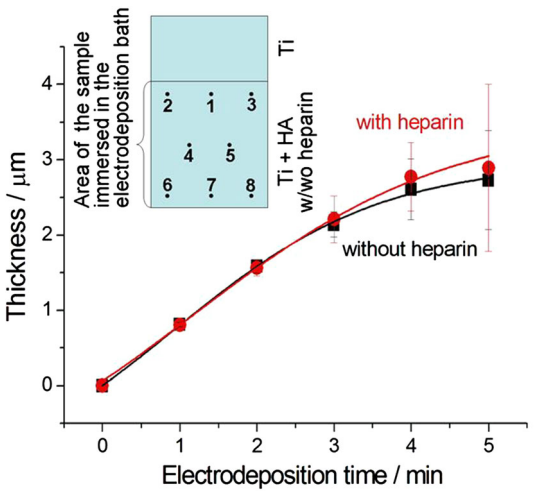

Fig. 1 Thickness of the coatings electrodeposited on titanium at −1.4 V versus Ag/AgCl from the solution containing $Ca(NO_3)_2$, $NH_4H_2PO_4$ and $NaNO_3$, with and without 1.7 g L^{-1} of heparin. Thickness data correspond to the mean ±1 standard deviation (SD) of data measured in eight points of the samples, schematically indicated in the inset. The lines are guides for the eye

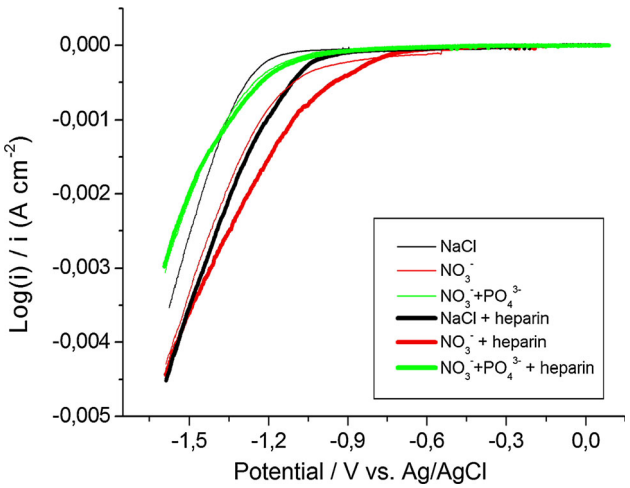

Fig. 2 Linear sweep voltammetries for Ti electrodes in contact with the following solutions: (*a*) = 0.1 M NaCl; (*b*) = 0.61 M $Ca(NO_3)_2$ and 0.1 M $NaNO_3$; (*c*) = 0.61 mM $Ca(NO_3)_2$, 0.1 M $NaNO_3$ and 0.36 mM $NH_4H_2PO_4$; (*d*) = solution (*a*) + 1.7 g L^{-1} heparin; (*e*) = solution (*b*) + 1.7 g L^{-1} heparin; (*f*) = solution (*c*) + 1.7 g L^{-1} heparin. Scan rate 1 mV s^{-1}

(i) 0.1 M NaCl; (ii) 0.1 M $NaNO_3$ and (iii) the full, calcium phosphate-containing solutions. The curve obtained from the NaCl solution shows that water reduction takes place at ca. −1.15 V. In the presence of NO_3^-, the shift of Tafel-type current density at less cathodic potentials indicates the combined effect of the reduction of water and nitrates. Instead, the addition of phosphates reveals the precipitation of HA, resulting in electrode passivation. The heparin added to the systems containing only NaCl or NO_3^- undergoes an electrochemical reaction, giving rise to an

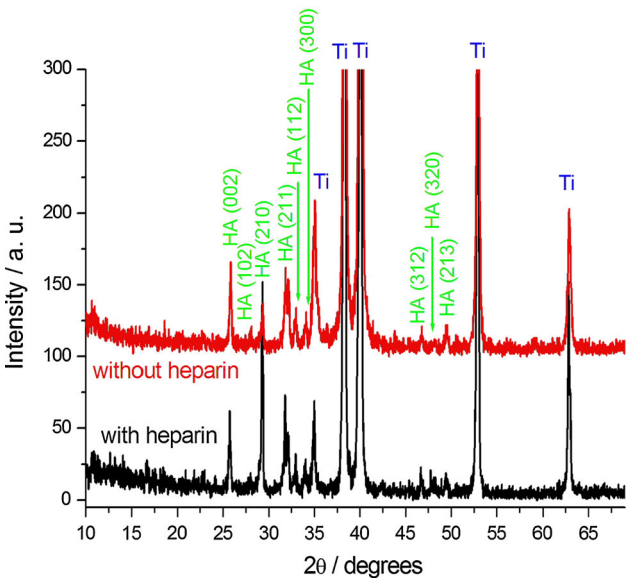

Fig. 3 X-ray diffractograms of HA coatings electrodeposited on titanium for 2 h at 1.4 V versus Ag/AgCl, at 100 °C from the solution containing 0.61 mM $Ca(NO_3)_2$, 0.1 M $NaNO_3$ and 0.36 mM $NH_4H_2PO_4$, in the absence and in the presence of 1.7 g L^{-1} heparin

increase of the current density. This effect however is not observed in the calcium phosphate electrodeposition bath: in fact the curves recorded in the presence and in the absence of heparin essentially overlap, indicating that heparin is readily isolated from electrochemically active sites of the electrode by the growing HA film.

3.2 Characterisation of the coatings

3.2.1 Crystallographic structure

Figure 3 shows X-ray diffractogram of the HA coatings electrodeposited on titanium under the optimal plating conditions in the absence and in the presence of heparin. The diffraction peaks can be readily indexed as standard HA patterns on titanium [2, 20, 21, 55, 56]. No other phases have been found to form by lowering the deposition temperature to 85 °C with N_2 bubbling and by varying the heparin concentration in the range 0/5 g L^{-1}. It is worth noting that our electrodeposition process is notably robust with respect to HA formation, at variance with the literature that reports the formation of HA only in a strictly controlled range of operating conditions [10, 13–15, 56].

3.2.2 Morphology

In Fig. 4 we report SEM micrographs of: (a) the pristine Ti surface; (b) HA electrodeposits grown for 2 h at −1.4 V at 85 °C from a bath deaerated by N_2 bubbling as well as (c) with the boiling solution and of HA-heparin complexes electrodeposited from boiling baths with different heparin

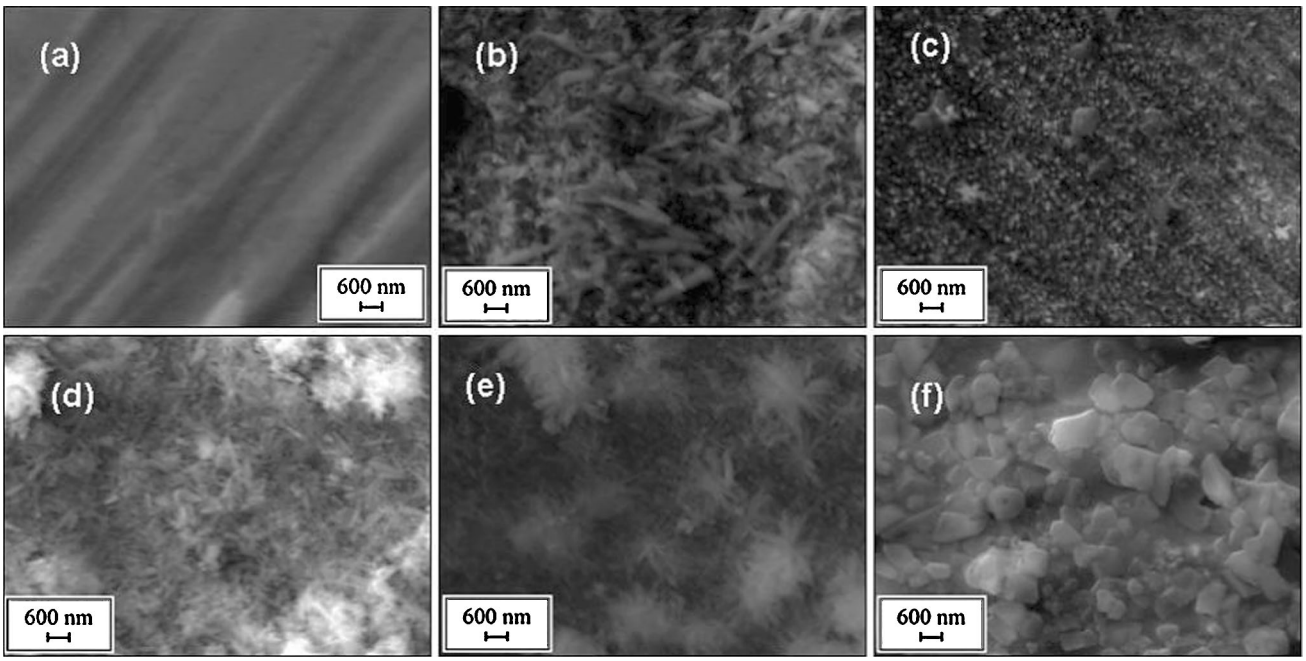

Fig. 4 SEM images of Ti surface before (**a**) and after HA electrodeposition at −1.4 V versus Ag/AgCl at 85 °C (**b**) and 100 °C (**c**) without heparin and at −1.4 V versus Ag/AgCl at 100 °C in the presence of different quantities of heparin: 0.5 (**d**), 1.7 (**e**) and 5.0 g L^{-1} (**f**)

concentrations: 0.5 (d), 1.7 (e) and 5.0 g L^{-1} (f). Panel (c) shows a nanostructure, that is desirable for bone mineralization [14]. Addition of heparin to the electrodeposition bath in the range 0.5/1.7 g L^{-1} (Panels d, e), leads to the formation of nanowires, that tend to assemble in globular structures as the heparin concentration increases. Optimal growth morphologies are thus obtained by using a boiling solution with heparin concentrations between 0.5 and 1.7 g L^{-1}. In fact, at the highest investigated heparin concentrations, a plate-like morphology develops, that is not suitable for the relevant applications (Panel f) since it largely diverges from the structural–functional organization of the natural bone (among others see e.g. [57–60], and literature cited therein). We also studied the electrode morphology resulting from the cathodic polarisation of Ti surfaces in the presence of heparin, but without HA precursors. Electrodeposition from a solution containing 0.1 M NaCl and 1.7 g L^{-1} heparin under otherwise identical conditions gives rise to the formation of a discontinuous film (Fig. 5).

3.2.3 Adhesion testing

Three replicates from each HA-coating were tested: the mean values and standard deviations are compiled in Table 1. Even though the shear test results on different coatings both without and with heparin are comparable, it is worth noting that, by increasing heparin content, the adhesion strength increases. The adhesion of HA-coatings was estimated by scratch tests: critical scratch loads for the tested experimental conditions are listed in Table 2. All samples exhibit ductile failure mechanisms and the obtained data are in close relationship with shear strength resistance (Fig. 6). The coating obtained from the bath with 1.7 g L^{-1} heparin is characterised by a series of nearly-circular microcracks, resulting from the tendency of the coating to conform to the scratch groove shape (Fig. 6, Panel b), thus resulting in the lowest level of critical scratch load. Microcracks depart from the scratch direction, according to the "conformal cracking" pattern defined by ASTM C 1624.

3.2.4 Qualitative and quantitative characterization of electrodeposited heparin

In order to confirm electrodeposition of a heparin-containing HA layer on Ti, samples grown in the optimal conditions were stained with Alcian Blue, a cationic dye that can be used for selective staining of glycosaminoglycans, such as heparin [45]. Alcian Blue staining was performed directly on a single titanium foil whose surface had been divided into three different areas by suitable masking: (i) uncoated, (ii) HA coated and (iii) HA-heparin coated (Fig. 7, Panel a). Light microscopy images of the stained titanium foils are shown in Fig. 7 Panels b, c. Only the HA-heparin coated surface binds the Alcian blue (Fig. 7, Panels a, b). Moreover, the staining is uniform (Fig. 7, Panel c), indicating effective and homogeneous coating of heparin all over the surface. The quantitative characterization of heparin on titanium

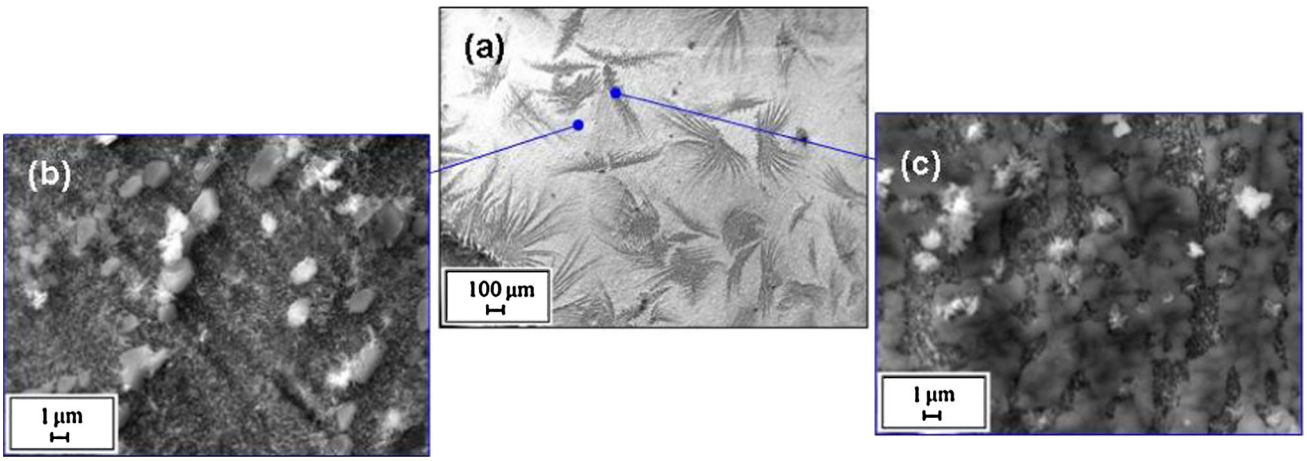

Fig. 5 SEM images of Ti surface after HA electrodeposition at −1.4 V versus Ag/AgCl and 100 °C from a solution containing 0.1 M NaCl and 1.7 g L^{-1} heparin

Table 1 Adhesion shear strengths of HA-coated Ti samples

Sample (substate + coating)	Mean shear strength (MPa)	Standard deviation (MPa)
Ti + HA (85 °C)	12.8	1.1
Ti + HA (100 °C)	16.3	0.8
Ti + HA 0.5 g L^{-1} heparin (100 °C)	10.4	1.6
Ti + HA 1.7 g L^{-1} heparin (100 °C)	11.9	2.1
Ti + HA 5 g L^{-1} heparin (100 °C)	17.5	1.9

Table 2 Critical scratch loads of HA-coated Ti samples

Sample (substate + coating)	Mean critical scratch load (*N*)	Standard deviation (*N*)
Ti + HA (85 °C)	7.67	0.58
Ti + HA (100 °C)	11.33	1.53
Ti + HA 0.5 g L^{-1} heparin (100 °C)	8.67	1.15
Ti + HA 1.7 g L^{-1} heparin (100 °C)	5.67	0.58
Ti + HA 5 g L^{-1} heparin (100 °C)	11.67	1.53

surface as a function of the heparin concentration used in the electrodeposition bath (0.2/5 g L^{-1}) was determined by the TBO assay (Fig. 7, Panel d). The amount of electrodeposited heparin was maximal using heparin concentration of 1.7 g L^{-1} in the electrodeposition bath (10.2 µg cm^{-2}). Overall, these results indicated the successful electrodeposition of heparin on Ti surface.

3.2.5 Cell proliferation and morphology

In order to assess cell proliferation/viability on the various surfaces, HeLa cell line was employed as cellular model. Cells were cultured on uncoated (control), HA coated and HA-heparin coated titanium surfaces for 48 h and proliferation was examined with the MTT assay (Fig. 8, Panel a). Cell viability was significantly higher on all the coated surfaces than on the control (pristine Ti) sample. Fluorescence microscopy images of the attached cells show uniform distribution and comparable morphology of the HeLa cells in the control sample (Fig. 8, Panel b) and HA (Fig. 8, Panel c) and HA-heparin (Fig. 8, Panel d) coated specimens.

4 Conclusions

In this investigation we have developed an electrochemical procedure for the direct potentiostatic electrodeposition of micrometer-thick HA-heparin composites as an improved osteointegration coating for Ti dental implants, with anticoagulant functionality. The bath chemistry has been optimised by singling out the electrochemical role of the individual components on the basis of linear sweep voltammetry measurements. By XRD we have demonstrated that single-phase HA can be reliably grown without special process-control requirements, both in the absence and in the presence of a wide range of heparin contents. SEM microscopy revealed that HA-heparin composites tend to grow in the form of nanowire structure: the morphology of choice for promoting bone ingrowth and osteointegration since e.g. it enhances the bioactivity for cell/tissue attachment, reinforces the osteoconductive properties of the scaffold and guides tissue growth (among others see e.g. [57–60], and literature cited therein). As the heparin concentration in the bath is increased, globular nanowire tangles develop, eventually merging into suboptimal plate-like structures for excessive heparin contents. Heparin

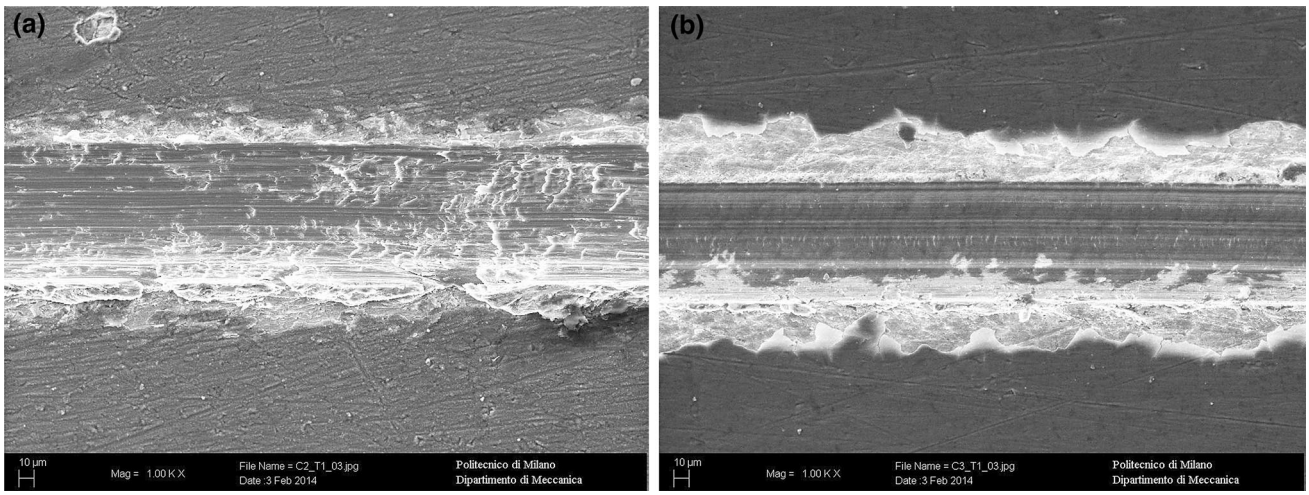

Fig. 6 Scratch test results of Ti samples coated with HA electrodeposited from baths containing heparin. **a** 0.5 g L^{-1}, **b** 1.7 g L^{-1}

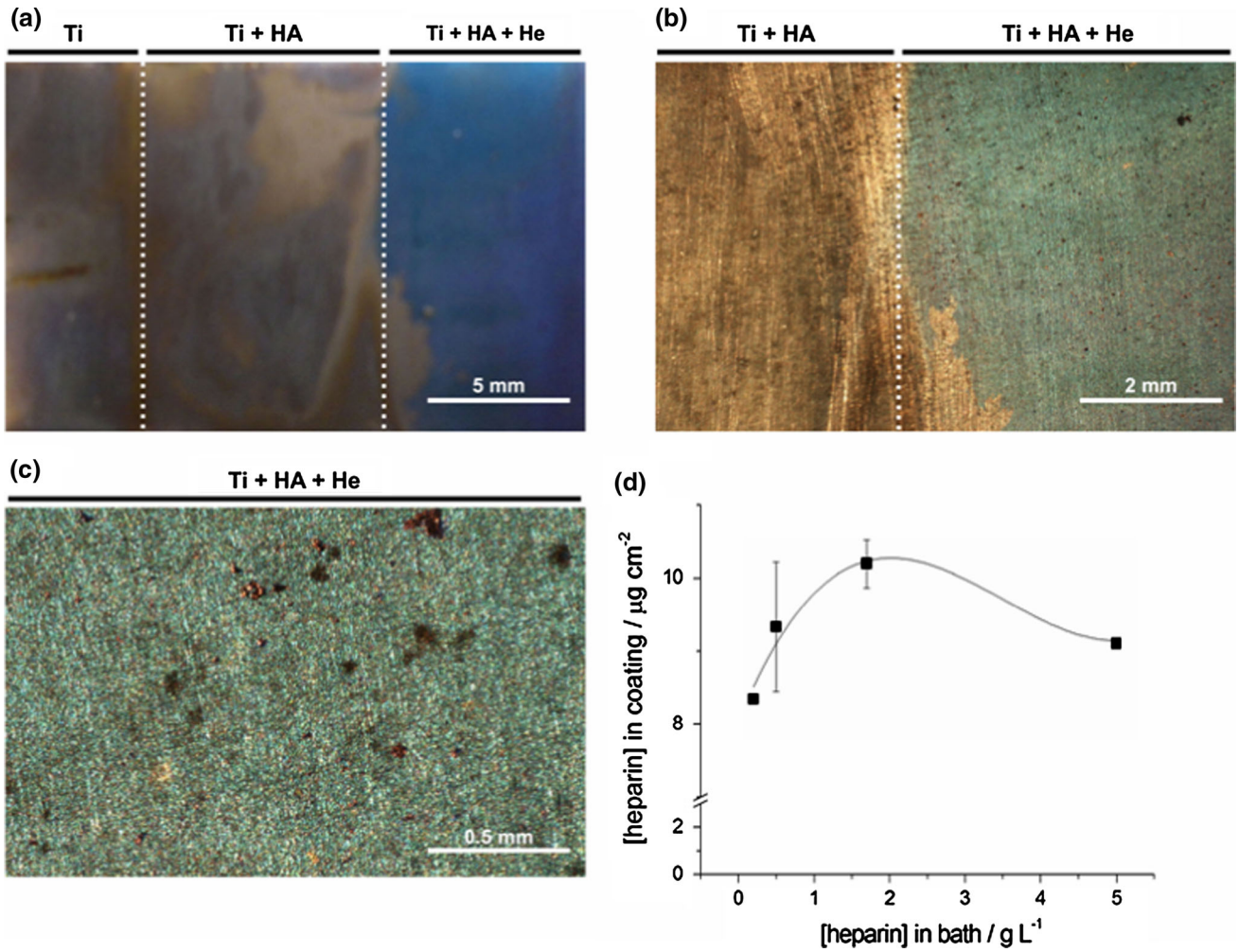

Fig. 7 Qualitative and quantitative characterisation of electrodeposited heparin. **a** Photographic image of Alcian Blue-stained titanium foil. The sample surface features uncoated-, HA coated- and HA-heparin coated-areas. **b**, **c** Light microscopy images of the Alcian Blue-stained titanium foil, **d** amount of heparin on HA-heparin coated titanium foils as a function of the heparin concentration used in the electrodeposition bath (0.2/5 g L^{-1}). The line is a guide for the eye

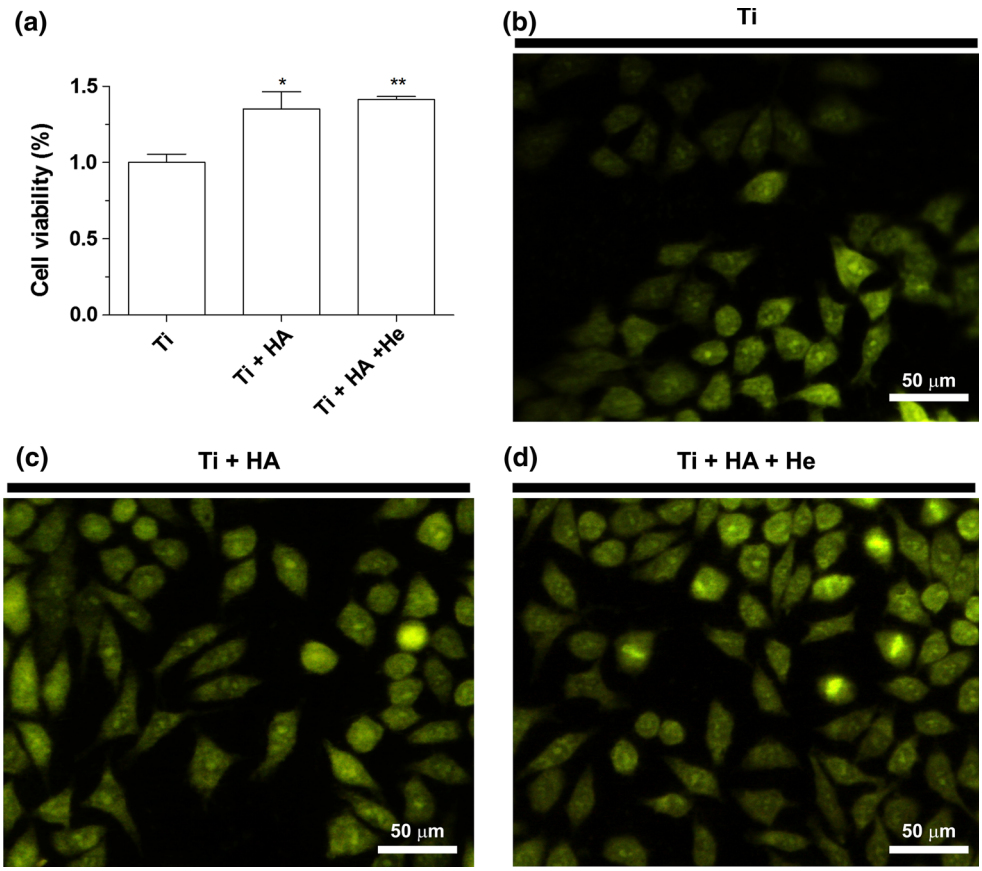

Fig. 8 **a** Viability of HeLa cells after 48 h of incubation on uncoated Ti surface (control) and the HA and HA heparin coated Ti foils. Data are expressed as percentage of control, and are represented by the mean ± standard error (SE) ($N = 3$ experiments). * and ** denoting $P < 0.05$ and $P < 0.01$, respectively (one way ANOVA analysis, Bonferroni post hoc test). **b–d** Fluorescence microscopy images of HeLa cells cultured on uncoated, HA coated and HA-heparin coated Ti surface, respectively

distribution in the composite coatings was assessed using Alcian Blue staining and found to be homogeneous. Heparin incorporation isotherms were measured by the TBO assay and an optimal concentration for the bath (1.7 g L^{-1}) was determined. The activity of the HA and HA-heparin coatings on Ti with respect to the proliferation/viability and morphology of HeLa cells were studied by MTT assay and fluorescence microscopy. Cell viability was found to be significantly lower on the bare Ti surface in comparison with HA and HA-heparin coatings: the latter material yielding a comparatively better performance, while cell morphology was unaltered.

References

1. Takebe J, Itoh S, Okada J, Ishibashi K. Anodic oxidation and hydrothermal treatment of titanium results in a surface that causes increased attachment and altered cytoskeletal morphology of rat bone marrow stromal cells in vitro. J Biomed Mater Res. 2000;51:398–407.
2. Kar A, Raja KS, Misra M. Electrodeposition of hydroxyapatite onto nanotubular TiO_2 for implant applications. Surf Coat Technol. 2006;201:3723–31.
3. Bozzini B, Carlino P, D'Urzo L, Pepe V, Mele C, Venturo F. An electrochemical impedance investigation of the behaviour of anodically oxidised titanium in human plasma and cognate fluids, relevant to dental applications. J Mater Sci Mater Med. 2008;19:3443–53.
4. Bozzini B, Carlino P, Mele C. Electrochemical behaviour and surface characterisation of Zr exposed to an SBF solution containing glycine, in view of dental implant applications. J Mater Sci Mater Med. 2011;22:193–200.
5. Jones JD, Lupori J, Van Sickels JE, Gardner W. A 5-year comparison of hydroxyapatite-coated titanium plasma–sprayed and titanium plasma–sprayed cylinder dental implants. Oral Surg Oral Med Oral Pathol. 1999;87:647–52.
6. Raja KS, Misra M, Paramguru K. Deposition of calcium phosphate coating on nanotubular anodized titanium. Mater Lett. 2005;59:2137–41.
7. Huang L, Xu K. A study of the process and kinetics of electrochemical deposition and the hydrothermal synthesis of hydroxyapatite coatings. J Mater Sci. 2000;11:667–73.
8. Zhu X, Son DW, Ong JL, Kim K. Characterization of hydrothermally treated anodic oxides containing Ca and P on titanium. J Mater Sci. 2003;14:629–34.
9. Chen JS, Juang HY, Hon MH. Calcium phosphate coating on titanium substrate by a modified electrocrystallization process. J Mater Sci Mater Med. 1998;9:297–300.
10. Manso M, Jiménez C, Morant C, Herrero P, Martìnez-Duart JM. Electrodeposition of hydroxyapatite coatings in basic conditions. Biomaterials. 2000;21:1755–61.
11. Kuo MC, Yen SK. The process of electrochemical deposited hydroxyapatite coatings on biomedical titanium at room temperature. Mater Sci Eng C. 2002;20:153–60.
12. Chen X, Zhao Z, Chen A, Li H. Pulsed electrodeposition of hydroxyapatite on titanium substrate in solution containing

hydrogen peroxide. Trans Nonferrous Metals Soc China. 2007;17:617–21.
13. Lin D-Y, Wang X-X. Electrodeposition of hydroxyapatite coating on CoNiCrMo substrate in dilute solution. Ceram Int. 2011;37:403–6.
14. dos Santos EA, Moldovan MS, Jacomine L, Matescu M, Werckmann J, Ansekme K, Mille P, Pelletier H. Oriented hydroxyapatite single crystals produced by the electrodeposition method. Mater Sci Eng B. 2010;169:138–44.
15. Shirkhanzadeh M. Direct formation of nanophase hydroxyapatite on cathodically polarized electrodes. J Mater Sci Mater Med. 1998;9:67–72.
16. Ban S. S. Maruno S. Hydrothermal–electrochemical deposition of hydroxyapatite. J Biomed Mater Res. 1998;42:387–95.
17. Kokubo T, Kim H-M, Kawashita M. Novel bioactive materials with different mechanical properties. Biomaterials. 2003;24:2161–75.
18. Lemma ED. Electrodeposition of hydroxyapatite for dental applications. MSc Thesis, Università del Salento, Italy; 2012.
19. Tanzi MC. Bioactive technologies for hemocompatibility. Expert Rev Med Devices. 2005;2:473–92.
20. Zhao DM, Wang YX, Chen ZY, Xu RW, Wu G, Yu DS. Preparation and characterization of modified hydroxyapatite particles by heparin. Biomed Mater. 2008;3:025016.
21. Sun F, Pang X, Zhitomirsky I. Electrophoretic deposition of composite hydroxyapatite–chitosan–heparin coatings. J Mater Process Technol. 2009;209:1597–606.
22. Hirsh J. Heparin. N Engl J Med. 1991;324:1565–74.
23. Weitz JI. Low-molecular weight heparins. N Engl J Med. 1997;337:688–98.
24. Hirsh J, Anand SS, Halperin JL, Fuster V. Guide to anticoagulant therapy: heparin. Circulation. 2001;103:2994–3018.
25. Baglin T, Barrowcliffe TW, Cohen A, Greaves M. Guidelines on the use and monitoring of heparin. Br J Haematol. 2006;133:19–34.
26. Young E. The anti-inflammatory effects of heparin and related compounds. Thromb Res. 2008;122:743–52.
27. Capila I, Linhardt RJ. Heparin—protein interactions. Angew Chem Int Ed. 2002;41:390–412.
28. Cornelius RM, Sanchez J, Olsson P, Brash JL. Interactions of antithrombin and proteins in the plasma contact activation system with immobilized functional heparin. J Biomed Mater Res A. 2003;67:475–83.
29. Ma R, Sask KN, Shi C, Brashc JL, Zhitomirsky I. Electrodeposition of polypyrrole-heparin and polypyrrole-hydroxyapatite films. Mater Lett. 2001;65:681–4.
30. Kim SE, Song SH, Yun YP, Choi BJ, Kwon IK, Bae MS, Moon HJ, Kwon YD. The effect of immobilization of heparin and bone morphogenic protein-2 (BMP-2) to titanium surfaces on inflammation and osteoblast function. Biomaterials. 2011;32:366–73.
31. Broggini N, Tosatti S, Ferguson SJ, Schuler M, Textor M, Bornstein MM, Bosshardt DD, Buser D. Evaluation of chemically modified SLA implants (modSLA) biofunctionalized with integrin (RGD)- and heparin (KRSR)-binding peptides. J Biomed Mater Res A. 2012;100:703–11.
32. Cacciatore P, Hallam K-R, Watkinson A-C, Allen G-C, Miles M-J, Jandt K-D. Visualisation of human plasma fibrinogen adsorbed on titanium implant surfaces with different roughness. Surf Sci. 2001;491:405–20.
33. Mustafa K, Wennerberg A, Wroblewski J, Hultenby K, Lopez BS, Arvidson K. Determining optimal surface roughness of TiO_2 blasted titanium implant material for attachment, proliferation and differentiation of cells derived from human mandibular alveolar bone. Clin Oral Implants Res. 2001;12:515–25.
34. Sul Y-T, Johansson C-B, Petronis S, Krozer A, Jeong Y, Wennerberg A, Albrektsson T. Characteristics of the surface oxides on turned and electrochemically oxidized pure titanium implants up to dielectric breakdown: the oxide thickness, micropore configurations, surface roughness, crystal structure and chemical composition. Biomaterials. 2011;23:491–501.
35. Rønold H-J, Lyngstadaas S-P, Ellingsen J-E. Analysing the optimal value for titanium implant roughness in bone attachment using a tensile test. Biomaterials. 2003;24:4559–64.
36. Rupp F, Scheideler L, Rehbein D, Axmann D, Geis-Gerstorfer J. Roughness induced dynamic changes of wettability of acid etched titanium implant modifications. Biomaterials. 2004;25:1429–38.
37. Wennerberg A, Albrektsson T, Andersson B. Bone tissue response to commercially pure titanium implants blasted with fine and coarse particles of aluminium oxide. Int J Oral Maxillofac Implants. 1996;11:38–45.
38. Wennerberg A, Albrektsson T. Implant surface beyon micron roughness. experimental and clinical knowledge of surface topography and surface. Int Dent. 2006;8:14–8.
39. Wennerberg A, Albrektsson T. On implant surfaces: a review of current knowledge and opinion. Int J Oral Maxillofac Implants. 2009;24:63–74.
40. Marcio Borges R, Albrektsson T, Francischone C-E, Schwartz Filho H-O, Wennerberg A. The influence of surface treatment in the implant roughness pattern. J Appl Oral Sci. 2012;20:550–5.
41. Ribarsky MW. Titanium Dioxide (TiO_2) (Rutile). In: Palik ED, editor. Handbook of optical constants of solids. Orlando: Academic Press; 1985. p. 795–800.
42. Inagaki M, Yokogawa Y, Kasmeyama T. Bond strength improvement of hydroxyapatite/titanium composite coating by partial nitriding during RF-thermal plasma sprying. Surf Coat Technol. 2003;173:1–8.
43. Albayrak O, El-Atwani O, Altintas S. Hydroxyapatite coating on titanium substrate by electrophoretic deposition method: effect of titanium dioxide inner layer on adhesion strength and hydroxyapatite decomposition. Surf Coat Technol. 2008;202:2482–7.
44. Gonzalez-McQuire R, Tsetsekou A. Hydroxyapatite-biomolecule coatings onto titanium surfaces. Surf Coat Technol. 2008;203:186–90.
45. Wissink MJ, Beernink R, Pieper JS, Poot AA, Engbers GH, Beugeling T, van Aken WG, Feijen J. Immobilization of heparin to EDC/NHS-crosslinked collagen. Characterization and in vitro evaluation. Biomaterials. 2001;22:151–63.
46. Smith PK, Mallia AK, Hermanson GT. Colorimetric method for the assay of heparin content in immobilized heparin preparations. Anal Biochem. 1980;109:466–73.
47. Mosmann T. Rapid colorimetric assay for cellular growth and survival: application to proliferation and cytotoxicity assays. J Immunol Methods. 1983;165:55–63.
48. Muller RH. Techniques for characterization of electrodes and electrochemical processes. New York: Wiley; 1991. p. 31–126.
49. Hassannejad H, Mele C, Shahrabi T, Bozzini B. Electrodeposition of Ni/ceria composites: an in situ visible reflectance investigation. J Solid State Electrochem. 2012;16:3429–41.
50. Stoica TF, Morosanu C, Slav A, Stoica T, Osiceanu P, Anastasescu C, Gartner M, Zaharescu M. Hydroxyapatite films obtained by sol–gel and sputtering. Thin Solid Films. 2008;516:8112–6.
51. Hemissi M, Amardjia-Adnani H. Optical and structural properties of titanium oxide thin films prepared by sol–gel method. Dig J Nanomater Biostruct. 2007;2:299–305.
52. Liu Y, Liu CY, Wei JH, Xiong R, Pan CX, Shi J. Enhanced adsorption and visible-light-induced photocatalytic activity of hydroxyapatite modified Ag-TiO2 powders. Appl Surf Sci. 2010;256:6390–4.
53. Santos O, Kosoric J, Hector MP, Anderson P, Lindh L. Adsorption behavior of statherin and a statherin peptide onto hydroxyapatite and silica surfaces by in situ ellipsometry. J Colloid Interf Sci. 2008;318:175–82.

54. de Araujo TS, de Souza SO, de Sousa EMB, Araujo MS. Production and thermal stability of pure and Cr^{3+}-doped hydroxyapatite. J Phys. 2010;249:012012.
55. Zhao X, Yang L, Zuo Y, Xiong J. Hydroxyapatite coatings on titanium prepared by electrodeposition in a modified simulated body fluid. Chin J Chem Eng. 2009;17:667–71.
56. Ye W, Wang XX. Ribbon-like and rod-like hydroxyapatite crystals deposited on titanium surface with electrochemical method. Mater Lett. 2007;61:4062–5.
57. Hu R, Lin CJ, Shi HY. A novel ordered nano hydroxyapatite coating electrochemically deposited on titanium substrate. J Biomed Mater Res A. 2006;80:687–92.
58. Chen F, Zhu YJ, Wang KW, Zhao KL. Surfactant-free solvothermal synthesis of hydroxyapatite nanowire/nanotube ordered arrays with biomimetic structures. Cryst Eng Commun. 2011;13:1858–63.
59. Zhao H, Dong W, Zheng Y, Liu A, Yao J, Li C, Tang W, Chen B, Wang G, Shi Z. The structural and biological properties of hydroxyapatite-modified titanante nanowire scaffolds. Biomaterials. 2011;32:5837–46.
60. Costa DO, Dixon SJ, Rizkalla AS. One- and three-dimensional growth of hydroxyapatite nanowires during sol–gel-hydrothermal synthesis. Appl Mater Interfaces. 2012;4:1490–9.